# *Ab initio* investigation of hybrid organic-inorganic perovskites based on tin halides

Ivo Borriello,* Giovanni Cantele, and Domenico Ninno
*Coherentia CNR-INFM and Università di Napoli "Federico II," Dipartimento di Scienze Fisiche, Complesso Universitario Monte Sant'Angelo, Via Cintia, I-80126 Napoli, Italy*
(Received 13 March 2008; revised manuscript received 7 May 2008; published 23 June 2008)

The structural and electronic properties of both inorganic and hybrid organic-inorganic perovskites based on tin halides are investigated from the first principles. In particular, we contrast the inorganic $CsSnCl_3$ and $CsSnI_3$ to their hybrid counterparts $(CH_3NH_3)SnCl_3$, $(CH_3NH_3)SnI_3$, and $(NH_2CH{=}NH_2)SnI_3$, which were obtained by substituting the inorganic Cs cation with the methylammonium $CH_3NH_3$ and the formamidinium $NH_2CH{=}NH_2$ cations. The comparison between the hybrid perovskites and the inorganic counterparts sheds light on the effects of the filling molecule on the structural and electronic properties of the compound. We show that the stability against the distortion of the perovskitic cage strongly depends on the embedded cation. The electronic properties (in particular, the band gap) can be tuned by a suitable choice of the organic molecule, and, in particular, of its size.

DOI: 10.1103/PhysRevB.77.235214 PACS number(s): 31.15.E−, 71.15.Mb, 71.20.Nr, 81.16.Dn

## I. INTRODUCTION

Hybrid organic-inorganic compounds are an emerging class of new materials that hold significant promise.[1–4] These complex structures, based on a molecular scale composite of organic and inorganic components, allow the combination of properties of organic and inorganic elements in a unique material. Inorganic compounds, typically characterized by covalent and ionic interactions, provide a wide range of electronic properties: high electrical mobility, wide range of band gaps (e.g., designing insulators, semiconductors, and metals), interesting magnetic and dielectric properties, thermal stability, and mechanical hardness. Organic compounds, which typically interact through weaker interactions (van der Waals or hydrogen bonding), offer the potential of high luminescence efficiency, large polarizability, plastic mechanical properties, and in some case exhibit conducting properties. Hybrid organic-inorganic compounds are considered innovative advanced materials. Promising applications are expected in many fields including optics, electronics, mechanics, protective coatings, catalysis, sensors, biology, and others.[1–18] The tuning of the electronic structure of hybrid materials at nanoscale can lead to unique electronic and optical properties that are typical neither of the organic nor of the inorganic component alone. This is the case of layered organic-inorganic heterostructures such as multiple quantum wells[10] (MQW), exhibiting a spatially modulated electronic structure. In particular, hybrid organic-inorganic multilayers realizing staggered[10,15] (or type II) MQW structures are of growing interest for their potential practical applications in electronic devices such as light-emitting diodes and photovoltaics.[11–18] The main working principle can be described as follows. Typically, electrons and holes are photogenerated in the organic layers, which absorb light in the visible region. The inorganic layers are selected to have high electron mobility, larger band gap, and larger electron affinity (compared to the organic layers). Electrons and holes are, thus, separated out at the organic-inorganic interface: the electrons transfer to the inorganic conduction band due to the larger electron affinity and the high electron mobility reduces the recombination probability, producing high photoconductivity gain.[15]

Hybrid perovskite compounds based on metal halides[4] are a particular class of organic-inorganic materials. The basic building component of the organic-inorganic perovskites is the $ABX_3$ perovskite structure. This simple structure consists of a network of corner-sharing $BX_6$ octahedra, where the B atom is a metal cation (typically $Sn^{2+}$ or $Pb^{2+}$) and X is a monovalent anion (typically $Cl^-$, $Br^-$, or $I^-$); the A cation is selected to neutralize the total charge and it can even be a molecule. In this case, the organic cation must fit into a rigid and relatively small cuboctahedral hole formed by the 12 nearest X atoms; thus, limiting the dimension of the selected molecule. In fact, a tolerance factor $t$ can be defined from the relation $(R_A+R_X)=t\sqrt{2}(R_B+R_X)$, where $R_A$, $R_B$, and $R_X$ are the ionic radii of the corresponding elements: by changing $R_A$, the tolerance factor $t$ can be varied but only in a restrict range of values around the unity ($t=1$ corresponds to a perfectly packed perovskite structure) to have a stable, even distorted, three-dimensional perovskite structure.[19] Perovskite based hybrids can be synthesized with simple and cheep techniques thanks to their self-assembling character.[20] The desired structural and electronic properties[21] can be engineered through a suitable choice of both the inorganic cage (that is, the B and X elements forming the $BX_6$ octahedra) and the cation. Moreover, the organic-inorganic superlattices are easily obtained by altering the combination of the organic and inorganic components in the starting solution from which the hybrids are crystallized. Therefore, the dimensionality can be used as a further degree of freedom for tuning the material properties. Inorganic layers [two-dimensional (2D) systems] or multilayers, as well as inorganic chains [one dimensional (1D)] and dots [zero dimensional] embedded in an organic matrix, have been fabricated.[8,22,23] For example, Mitzi *et al.* have demonstrated that layered perovskites with unit formula $[NH_2C(I){=}NH_2]_2(CH_3NH_3)_mSn_mI_{3m+2}$ can be synthesized to realize 1D ($m=1$), 2D ($m=2$), or multilayer ($m>2$) inorganic structures, which have different conductivities.[8,23] For all these and other reasons, metal (in particular, lead and tin) halide hybrid perovskites have been extensively studied in

 

the last 20 years.[21,24–54] In this framework, *ab initio* investigations are used to shed light on the links between the structure, chemical composition, and properties, offering the possibility of designing new functional structures with the desired characteristics.

Our attention has been focused on $ASnX_3$ perovskites. For such compounds, distorted tin environments are typically detected in the low-temperature phase due to the presence of stereochemically active electron lone pair on tin.[55] The distortion of the octahedra is found to be significantly reduced upon decreasing the electronegativity of the X ligand halogen. These general structural observations are rationalized, within the LCAO model, by the simple concept of "orbital energy matching" between the appropriate halogen group orbital and the tin bonding orbital: the latter rises from a suitable combination of 5*s* and 5*p* tin orbitals as to match the energy of the halogen *np* orbital. Depending on the halogen, a different mixture of 5*s* and 5*p* orbitals occurs, resulting in a different bond directionality or, equivalently, a distortion of the $SnX_6$ octahedra.[55] Moreover, many $ASnX_3$ compounds have an undistorted perovskite structure in the high-temperature phase. The structural phase transition may induce significant changes on the electronic properties. Finally, the structural and electronic properties may strongly depend on the choice of the cation.[21,42]

In this paper, the first-principles calculations of $ASnX_3$ crystals with $A=[Cs, CH_3NH_3(MA), NH_2CH=NH_2(FO)]$ and $X=[Cl, I]$ are presented: the structural and electronic properties of these compounds are analyzed and related to the particular choice of both the X halogen and the A cation embedded in the corner-sharing $BX_6$ octahedra network. Different structural phases are considered, and the variation of the optical and electronic properties induced by the transition from high-to low-temperature phases is elucidated. Moreover, an explicit comparison between the hybrid organic-inorganic and the inorganic perovskites is made by replacing the inorganic Cs cation with the methylammonium (MA) and formamidinium (FO) organic molecules. The size of the embedded organic cation is reflected on the volume of the cubic inorganic cage that, as it will be shown, can in turn be used for engineering the energy gap.

The paper is organized as follows. In Sec. II, we summarize the technical details of the calculations. The results concerning the structural and electronic properties of both inorganic and hybrid organic-inorganic compounds are discussed and compared with the experimental measurements in Sec. III. Finally, in Sec. IV, some conclusions are drawn.

## II. METHOD

We have performed *ab initio* calculations in the framework of density functional theory, as implemented in the Quantum-ESPRESSO package,[56] based on a plane-wave basis set for the expansion of the single-particle Kohn–Sham wave functions and pseudopotentials to describe the computationally expensive electron–ion interaction. Vanderbilt-type ultrasoft pseudopotentials[57] have been used to represent all atoms except for Iodine (I) and Cesium (Cs), for which a Troullier–Martin[58] norm-conserving pseudopotential has been selected. The generalized gradient approximation was employed for the evaluation of the exchange-correlation energy. The electronic wave functions have been expanded using plane waves corresponding to energies up to 30 Ry while a 180 Ry cutoff energy has been used to represent the total charge density. A $4\times4\times4$ Monkhorst–Pack grid[59] has been chosen for sampling the Brillouin zone. For all the considered structures, the theoretical optimal lattice parameters have been estimated. The x-ray diffraction data (where available) were used as a starting point for the optimization of the crystal structures. The full relaxation of the atomic positions within the unit cell is allowed following the Broyden–Fletcher–Goldfarb–Shanno algorithm. We carefully checked the convergence of the calculated properties with respect to the calculation parameters.

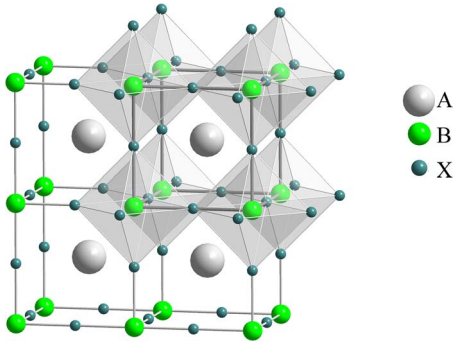


FIG. 1. (Color online) The basic $ABX_3$ perovskite structure. The $BX_6$ corner-sharing octahedra are evidenced.

## III. RESULTS AND DISCUSSIONS

$ASnX_3$ crystals exhibit a cubic perovskite structure in the highest temperature phase. Figure 1 shows the basic unit, which consists of corner-linked octahedra of the X anions, with the B cation at their center, and the A cation between them. As observed for most of the inorganic perovskitic structures,[60] $ASnX_3$ exhibits, as a function of the temperature, phase transitions characterized by (i) the deformation (typically referred to as distortion) of the octahedra, (ii) the displacement of the inorganic A cation, (iii) the tilting of the corner-sharing octahedra network, or (iv) all of them.

In the following, we will refer to a distorted (or deformed) network in the presence of deviations from the regularity of the octahedra. In contrast, we will refer to a tilted network in the presence of relative displacements (rotations) of the octahedra with respect to the ideal perovskite structure. The tilting can be quantified in the case of an almost regular (not deformed) octahedra network through the bridging angles B-X-B. A schematic view is given in Fig. 2 in the case of an orthorhombic $ABX_3$ structure where two tilting angles can be defined: $\Theta_{ab}$ in the *ab* plane and $\Theta_c$ along the *c* axis.

For $CsSnX_3$ inorganic perovskites, the changes of the electronic properties (i.e., electronic conductivity and optical absorption), resulting from phase transitions, are mainly described by structural variations (deformation and tilting) of the octahedra and dramatically depend on the choice of the X halogen, as evidenced by the two limiting cases X=Cl and

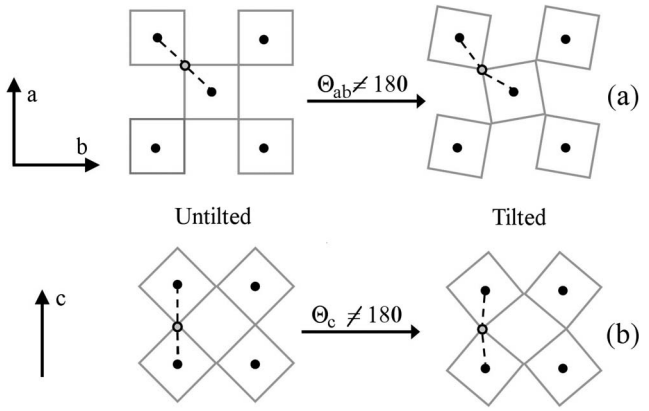


FIG. 2. Tilting angles for an $ABX_3$ structure. The (untilted) cubic configuration (left) is compared to the (tilted) orthorhombic one (right) in (a) the *ab* plane and (b) along the *c* axis. The octahedra are represented by squares with B atom (black circle) at the center. The X atom at the square corner (gray circle) is evidenced to visualize the bridging angle.

X=I. The replacement of the inorganic cation with a suitable organic molecule produces tunable changes of the structural and electronic properties with respect to the corresponding inorganic compound. To shed light on this point, we first analyze the $CsSnX_3$ compounds (with X=I and Cl) and then their hybrid counterparts.

### A. Electronic properties of $CsSnI_3$

Upon lowering the temperature, the $CsSnI_3$ compound undergoes two phase transitions:[61] *cubic* (I) $\overset{T=426\ \mathrm{K}}{\rightarrow}$ *tetragonal* (II) $\overset{T=351\ \mathrm{K}}{\rightarrow}$ *orthorhombic* (III). *Ab initio* structural parameters of the fully relaxed system are reported in Table I. The theoretical results are in good agreement with the structural experimental data reported by Yamada[61] *et al.* The cubic phase of $CsSnI_3$ (or phase I) is characterized by a perfect perovskitic structure (Fig. 1) with regular $SnI_6$ octahedra aligned along the three directions of the cubic lattice. The transition to the tetragonal phase (or phase II) is accompanied by a tilt of the octahedra in the *ab* plane (Fig. 3), the unit cell volume is nearly doubled (in particular, the *a* lattice parameter is about $\sqrt{2}$ times the value of the lattice constant of cubic phase) and two $CsSnI_3$ units form the basis inside the unit cell. The six I halogens at the corners of the octahedra are at nearly the same distance from the Sn atom (with a mean value of 3.136 Å and a maximum difference of 0.01 Å between each other). No deformation of the octahedra occurs (the internal angles of each octahedron are exactly 90°).

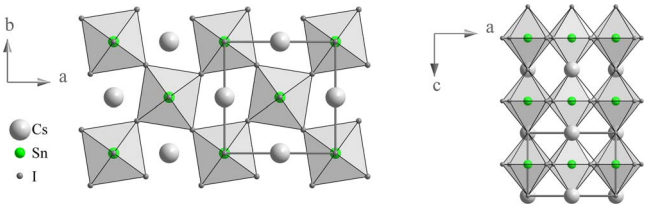


FIG. 3. (Color online) A perspective of $CsSnI_3$ in the tetragonal phase (II). The tilting of the octahedra is in the *ab* plane (left panel), whereas no tilt occurs along the *c* axis (right panel). The unit cell is sketched for clarity.

The regularity of octahedra allows the establishment of tilting angles by looking at the iodine bridging angles Sn-

TABLE I. Calculated energy gap $E_g$ (in eV) and crystallographic parameters *a*, *b*, and *c* (in Å), and $\alpha$, $\beta$, and $\gamma$ (in degrees) for the $ABX_3$ perovskites investigated in this work. *N* is the number of structural units in the unit cell. The experimental results, where available, are reported in parentheses. A maximum deviation of 3% is found between the computed and measured *a* parameter of $CsSnCl_3$ (II).

| $ASnX_3$ | *a* | *b* | *c* | $\alpha$ | $\beta$ | $\gamma$ | N | $E_g$ |
|---|---|---|---|---|---|---|---|---|
| $CsSnI_3$ (I) | 6.231 | - | | - | - | - | 1 | 0.348 |
| | (6.219) | | | | | | | |
| $CsSnI_3$ (II) | 8.772 | - | 6.261 | - | - | - | 2 | 0.481 |
| | (8.772) | | (6.261) | | | | | |
| $CsSnI_3$ (III) | 8.738 | 12.528 | 8.73 | - | - | - | 4 | 0.561 |
| | (8.688) | (12.378) | (8.643) | | | | | |
| $CsSnCl_3$ (I) | 5.601 | - | - | - | - | - | 1 | 0.950 |
| | (5.604) | | | | | | | |
| $CsSnCl_3$ (II) | 16.672 | 7.735 | 5.768 | - | 92.8 | - | 4 | 2.845 |
| | (16.10) | (7.425) | (5.748) | | (93.2) | | | |
| $MASnCl_3$ (IV) | 5.888 | 8.381 | 8.013 | 90.2 | 96.1 | 89.9 | 2 | 1.957 |
| | (5.726) | (8.277) | (7.910) | (90.4) | (93.08) | (90.15) | | |
| $MASnI_3$ (I) | 6.286 | - | - | - | - | - | 1 | 0.468 |
| | (6.242) | | | | | | | |
| $FOSnI_3$ (I) | 6.396 | - | - | - | - | - | 1 | 0.698 |
| | (6.316) | | | | | | | |

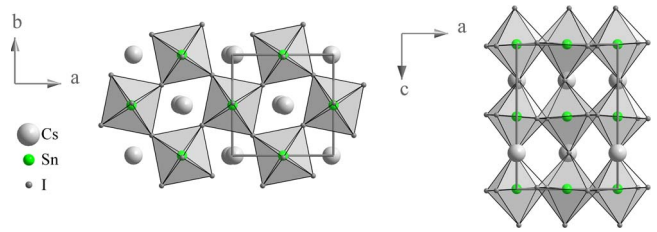


FIG. 4. (Color online) A perspective of $CsSnI_3$ in the orthorhombic phase (III). In the left (right) panel, it is shown that the tilting of the octahedra in the *ab* (*ac*) plane. The unit cell is sketched for clarity.

I-Sn in the *ab* plane ($\Theta_{ab}$) and parallel to the *c* axis ($\Theta_c$). Flat angles correspond to perfectly aligned Sn-I-Sn chains, as in the case of perfect cubic perovskites (see Fig. 1).

As shown in Fig. 3, in the tetragonal phase, no tilt occurs along the *c* axis ($\Theta_c$=180°), whereas the octahedra network is tilted in the *ab* plane ($\Theta_{ab}$=162°), corresponding to the mutual rotation around the *c* axis of adjacent $SnI_6$ octahedra by 9° in opposite directions.

In Fig. 4, the orthorhombic phase (or phase III) is shown: the unit cell increases further two times along the *c* axis, thus containing four $CsSnI_3$ units. The Sn-I distances in the octahedron are almost of the same length (with a mean value of 3.146 Å and a maximum difference of 0.03 Å between each other), whereas the internal angles now differ at most of 0.5° from 90°, thus leading us to also consider the orthorhombic phase as constituted by a regular octahedra network. This means that, also in this case, we can relate the tilting of the octahedra to the Sn-I-Sn bridging angles. $\Theta_{ab}$ is almost the same as for the tetragonal phase while a tilt appears along the *c* axis ($\Theta_c$=173°). It is interesting to note that the two phase transitions do not significantly affect the octahedron internal structure [the mean value of Sn-I lengths varies from 3.115 (phase I) to 3.146 Å (phase III)]. On the other hand, they result in a progressive increase in the tilting of the octahedra network.

The electronic band structure, the density of states (DOS), and the projected density of states (PDOS) of $CsSnI_3$ are shown in Fig. 5. The left panel is associated with the orthorhombic phase or phase III, the central panel to the phase II, and the right one to the phase I. The calculated band structure and the total DOS for each phase (the gray shadows on the left) is reported in Fig. 5(a). The zero energy is arbitrarily set to the valence band maximum (VBM). *N* is the number of $CsSnI_3$ units inside the unit cell. The DOS and the PDOS (see Fig. 5) are opportunely scaled by *N* to make a clear comparison among different phases.

The projection is done onto the atomic orbitals of each atom.

In Fig. 5(b), the contribution of Sn *s* and *p* orbitals to the total DOS is shown along with the total contribution of I atoms and Cs cation. Similarly, in Fig. 5(c), the contribution of the I *s*, *p*, and *d* orbitals to the DOS is represented along with the total contribution of Sn and Cs. From the band structure calculation, a direct band gap is found for all the phases of $CsSnI_3$ (at *R*, *Z*, and Γ points of the Brillouin zone for phases I, II, and III, respectively). A gradual increase in the band gap (see Table I) is observed by following the series of phase transitions in the order I→II→III, that is, upon increasing the tilting of the octahedra network. Moreover, the direct band gap is in correspondence of a sharp maximum in the electronic valence band while a rapid lowering of the DOS approaching the VBM value is found. An overall similarity between the PDOS of all the phases is found: the valence band is mostly dominated by I *p* orbital contributions; whereas in the near band-gap energy region, the conduction

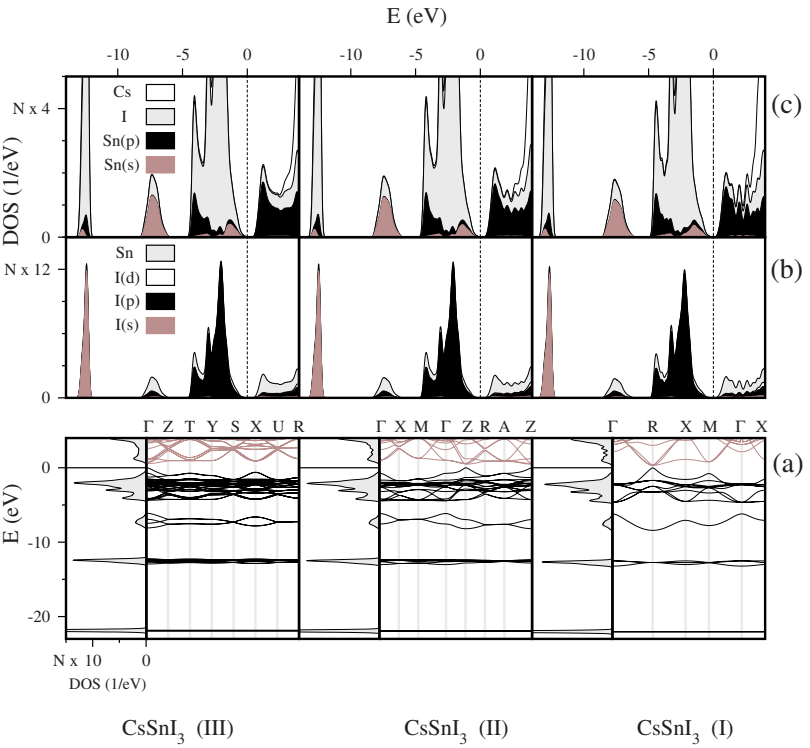


FIG. 5. (Color online) Calculated electronic properties of the different phases of $CsSnI_3$: (a) band structure (Ref. 62) and total DOS; (b) PDOS on Sn (all orbitals), and I *s*, *p*, and *d* orbitals; (c) PDOS on Cs (all orbitals), I (all orbitals), and Sn *s* and *p* orbitals. The VBM is arbitrarily set to zero. In (a), the filled (empty) bands are indicated with black (brown) lines.

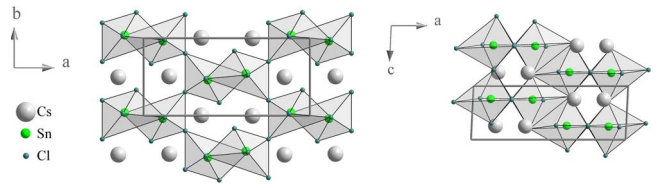


FIG. 6. (Color online) A perspective of the monoclinic phase (II) of $CsSnCl_3$ in the *ab* plane (left panel) and in the *ac* plane (right panel). The unit cell is evidenced for clarity.

band is essentially dominated by Sn *p* orbitals with a slight contribution of I *p* orbitals. Moreover, a slight superposition of Sn (*s* and *p*) with I (*p*) PDOS is found below the VBM (between −5 and 0 eV), thus suggesting a partial hybridization of the Sn-I bond. Sn *p* states mostly contribute to bands above the VBM, supporting the ionic character of the compound.

### B. Electronic properties of $CsSnCl_3$

Upon lowering the temperature, the $CsSnCl_3$ compound undergoes just one phase transition:[42] *cubic* (I) $\overset{T=359\ K}{\rightarrow}$ *monoclinic* (II). A good agreement between the computed and the measured[63] structural parameters is found for both phases, as shown in Table I. In the cubic phase, the $CsSnCl_3$ compound exhibits a perfect perovskitic structure (Fig. 1) with a regular untilted octahedra network. The transition to the monoclinic phase is characterized by a dramatic change of the structural properties of the compound, as clearly shown in Fig. 6. The octahedra are strongly deformed: the Sn-Cl distances in the $SnCl_6$ octahedron are in agreement with the results reported by Yamada *et al.*[42] According to their findings, in this phase the octahedron is constituted by $SnCl_3^-$ anions, which form a trigonal pyramid (Sn-Cl bonds: 2.54, 2.57, and 2.62 Å) having three long interanionic interactions (Sn-Cl distances: 3.15, 3.49, and 4.07 Å).

Moreover, a transition from a corner-sharing octahedra network (Fig. 1) to an edge-sharing octahedra chain network is observed (Fig. 6). The octahedra chains, parallel to the *c* axis, are separated from each other by Cs cations along the *a* and *b* axes. As a consequence of the breaking of the corner-sharing octahedra network, the Cs cation is no longer embedded in a pseudocubic cage with Sn atoms at the vertex (Fig. 6).

The electronic band structure and the DOS of $CsSnCl_3$ are shown in Fig. 7 (left and central panels) following the same scheme as Fig. 5. At variance with $CsSnI_3$, the phase transition dramatically changes the electronic properties of the compound. A much wider band gap (at *D* point) shows up (Table I), the sharp maximum in the valence band disappears, and a different behavior of the DOS approaching to the VBM is found. Moreover, the bands are almost exclusively dispersed along the *z* direction of the Brillouin zone ($C \rightarrow Y$, $B \rightarrow D$, $E \rightarrow Y$, and $\Gamma \rightarrow Z$ segments in the path of Fig. 7). The bands are indeed nearly flat elsewhere. This effect is due to the breaking of the corner-sharing 3D octahedra network with the formation of almost isolated edge-sharing octahedra chains. As a consequence, the bands are dispersed mainly along the chain direction. In analogy with the cubic phase, the valence band is dominated by Cl *p* orbitals; whereas, in the near band-gap energy region, the conduction band is dominated by the Sn *p* orbitals with a minor admixture from the Cl *p* states.

### C. $CH_3NH_3SnCl_3$ in the low-temperature phase

Upon decreasing the temperature, the $CH_3NH_3SnCl_3$ compound undergoes three phase transitions:[42]

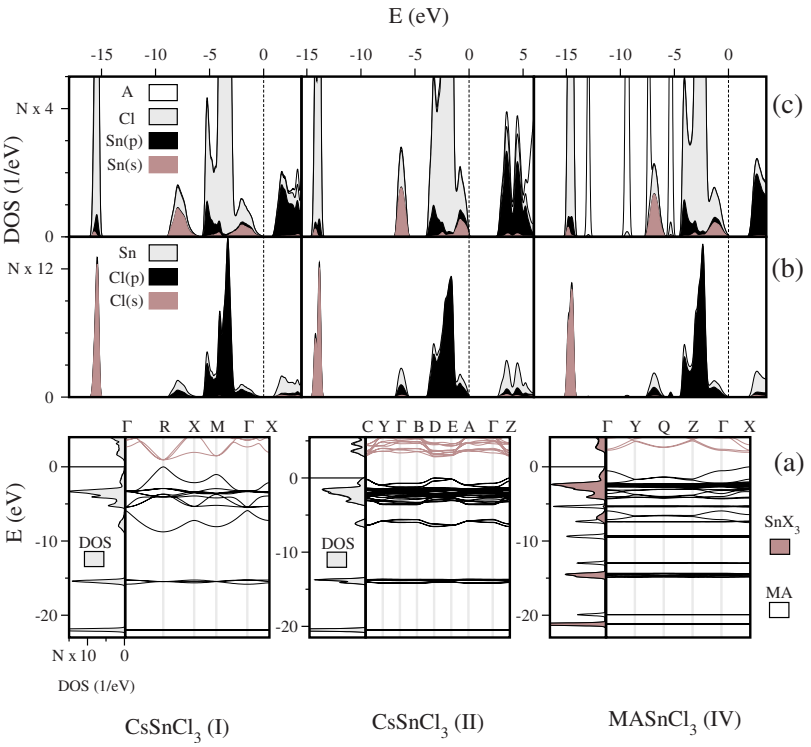


FIG. 7. (Color online) Calculated electronic properties of $CsSnCl_3$ (phases I and II) and of $MASnCl_3$ (phase IV): (a) band structure (Ref. 62) and total DOS ; (b) PDOS on Sn (all orbitals), and Cl *s* and *p* orbitals; (c) PDOS on all A (A =Cs,MA) orbitals, all Cl, and all Sn *s* and *p* orbitals. The VBM is arbitrarily set to zero. In (a), the filled (empty) bands are indicated with black (brown) lines. The total DOS of $MASnCl_3$ (on the left of the band structure) is decomposed into organic (white) and inorganic (brown) contributions.

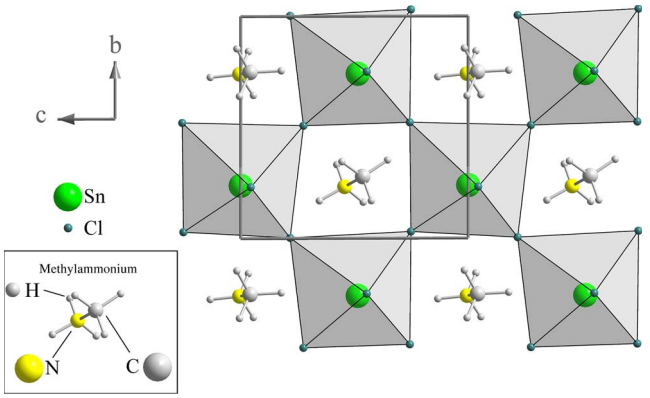


FIG. 8. (Color online) A perspective on the *bc* plane of $CH_3NH_3SnCl_3$ in the triclinic phase. The unit cell is evidenced for clarity.

*cubic* (I) $\xrightarrow{T=463\ \mathrm{K}}$ *rhombohedral* (II) $\xrightarrow{T=331\ \mathrm{K}}$ *monoclinic* (III) $\xrightarrow{T=307\ \mathrm{K}}$ *triclinic* (IV). In the high-temperature phases (I and II), (mostly) regular perovskitic cages embed the MA $CH_3NH_3^+$ cations, which are believed to be dynamically disordered[42] (random orientation). The dynamical disorder disappears on cooling: in the low-temperature phases (III and IV), an ordered orientation of the MA cations shows up. It can be described in terms of potential wells (for the $NH_3^+$ polar head) that originate from the distortions of the $SnCl_6$ octahedra.

We focus on the triclinic phase and compare the structural and electronic properties of the low-temperature phase of $MASnCl_3$ to those of its inorganic counterpart (see Sec. III B). The *ab initio* structural parameters of the fully relaxed system are reported in Table I, showing a fair agreement with the experimental data.[42] A perspective of the phase IV of $MASnCl_3$ is shown in Fig. 8 to be contrasted to Fig. 6 (low-temperature phase of the inorganic counterpart $CsSnCl_3$). Much less pronounced deformations of the octahedra are found in this case. The presence of methylammonium (in contrast to Cs) allows the inorganic cage to preserve a corner-sharing octahedra network structure in the low-temperature phase. The octahedra are not regular: the $SnCl_3^-$ anions form a trigonal pyramid (Sn-Cl bonds: 2.57, 2.65, and 2.7 Å) having three long interanionic interactions (Sn-Cl distances: 3.14, 3.22, and 3.37 Å), in analogy with the $CsSnCl_3$.

The band structure of the triclinic $MASnCl_3$ is represented in Fig. 7. The direct band gap is at the X point, in correspondence to a fairly sharp maximum of the valence band. Interestingly, the band gap is lower than that of the inorganic counterpart in the low-temperature phase. The PDOS reveals that the organic cation only contributes to the flat bands, whereas no cation contribution to the dispersed bands of the near band-gap region comes out. Because no hybridization occurs between the orbitals for the organic and inorganic components, the preservation of the corner-sharing octahedra network structure in the low-temperature phase can be attributed to the steric interaction between the inorganic cage and the organic cation due to the large size of the latter.

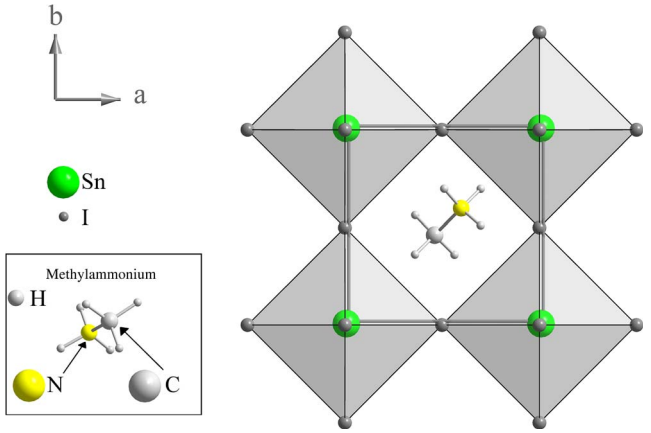


FIG. 9. (Color online) A perspective of $CH_3NH_3SnI_3$ in the cubic phase. The unit cell is sketched for clarity.

### D. Electronic properties of $ASnI_3$ with A=($CH_3NH_3$, $NH_2CH=NH_2$)

In analogy with the inorganic $CsSnI_3$, the hybrid $ASnI_3$ (A=MA,FO) adopts a cubic perovskite structure in the highest temperature phase (room temperature[41]). Mitzi and Liang[41] measured the room temperature x-ray powder patterns demonstrating the isostructural relationship between the two compounds and the increase in the cubic lattice parameter when the smaller MA cation is replaced by the FO cation.

Some points should be highlighted here: (i)in the cubic perovskite structure, the tilting of the corner-sharing octahedra network is forbidden by the symmetry of the crystal[64] (whose space group is *Pm3m*); (ii) in this phase, the substitution of the inorganic Cs (spherical ion) with the organic MA and FO produces only a very slight deformation of the octahedra,[45] accompanied by a dynamical disorder of the molecules, as inferred from the absence of x-ray diffraction patterns of the organic cations.[25,27–30,33,34,39,42,44,46]

It should be remarked that, in our calculations, the molecule is fixed at the minimum energy configuration. Under this constrain (*fixed orientation*), it is expected that the computed $ASnI_3$ cubic perovskitic structures would present, at most, a higher deformation of the octahedra with respect to the real crystal (which is characterized by an *isotropic orientation* of the organic cations). On the other hand, our results on $CsSnX_3$ (X=Cl,I) indicate that the iodine assures the formation of almost regular $SnI_6$ octahedra (the different phase transitions of $CsSnI_3$, in contrast to Cl, produce only the tilting of the octahedra network with negligible deformation effects). This observation suggests that, even if the molecule is fixed, the calculated crystal structure of $ASnI_3$ in the cubic phase would exhibit a mostly regular perovskitic structure in agreement with the experimental results.[41]

The lattice parameters of the cubic $MASnI_3$ and $FOSnI_3$ obtained from fully relaxed geometry are reported in Table I, which is again in a good agreement with the experimental data.[41] The relaxed structures are shown in Figs. 9 and 10. In both compounds, a mostly regular perovskitic cage embeds the organic molecule with slight deformations of the $SnI_6$ octahedra. The octahedra deformation increases upon in-

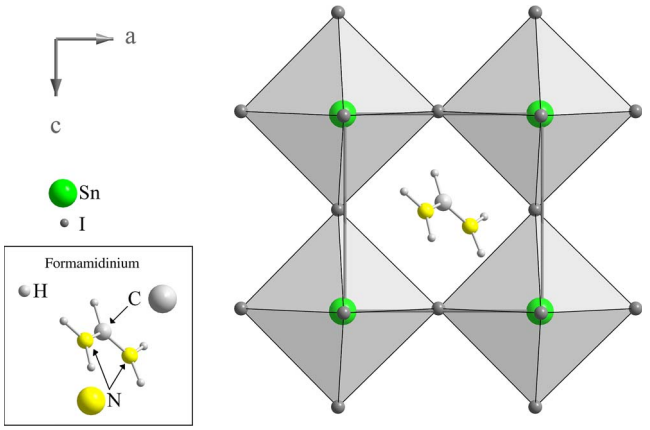


FIG. 10. (Color online) A perspective of $NH_2CH{=}NH_2SnI_3$ in the cubic phase. The unit cell is sketched for clarity.

creasing the molecule size, that is, by substituting the smaller MA cation with FO. The band structures of $MASnI_3$ and $FOSnI_3$ are represented in Fig. 11(a). For both compounds, the direct band gap (see Table I) is at the *R* point, in correspondence of a sharp maximum in the valence band. Moreover, the organic contributions to the total DOS are in correspondence to the flat bands (molecular orbitals) that are far from the near band-gap region. In the band-gap energy region, the valence and conduction bands are dominated by the inorganic cage, instead.

### E. Role of the organic cation

As it emerges from the PDOS of all the considered compounds, the near band-gap energy region is dominated by the inorganic network contributions, which raises the question on how the choice of the cation embedded in the inorganic $SnX_3$ cage can modify the electronic properties (e.g., the band gap) of these compounds. To answer this question, some observations have to be made.

An interesting result is shown in Fig. 12. The band gap of the hybrid organic-inorganic $ASnI_3$ compounds is very close to that of a hypothetical $CsSnI_3$ cubic perovskite with the same cell size. The very small difference arises from the slight deformation of the octahedra in the hybrid perovskites. Thus, the molecule plays the role of an electron donor exactly like the inorganic cation but also determines the size of the cell. In Fig. 12, the energy band-gap values of the tetragonal (phase II) and orthorhombic (phase III) of $CsSnI_3$ are also reported: the network tilting in the low-temperature phases of $CsSnI_3$ results in an increasing of the band gap. This means that the band gap is very sensitive to any modification (enlargement, tilting, and/or deformation) of the octahedra network.

By looking at the $MASnCl_3$ and $CsSnCl_3$, we found that the transition to the low-temperature phase causes, in the latter, the breaking of the corner-sharing octahedra network with a dramatic increasing of the band gap (see Table I). Interestingly, the low-temperature phase of the hybrid $MASnCl_3$ preserves the octahedra network structure and,

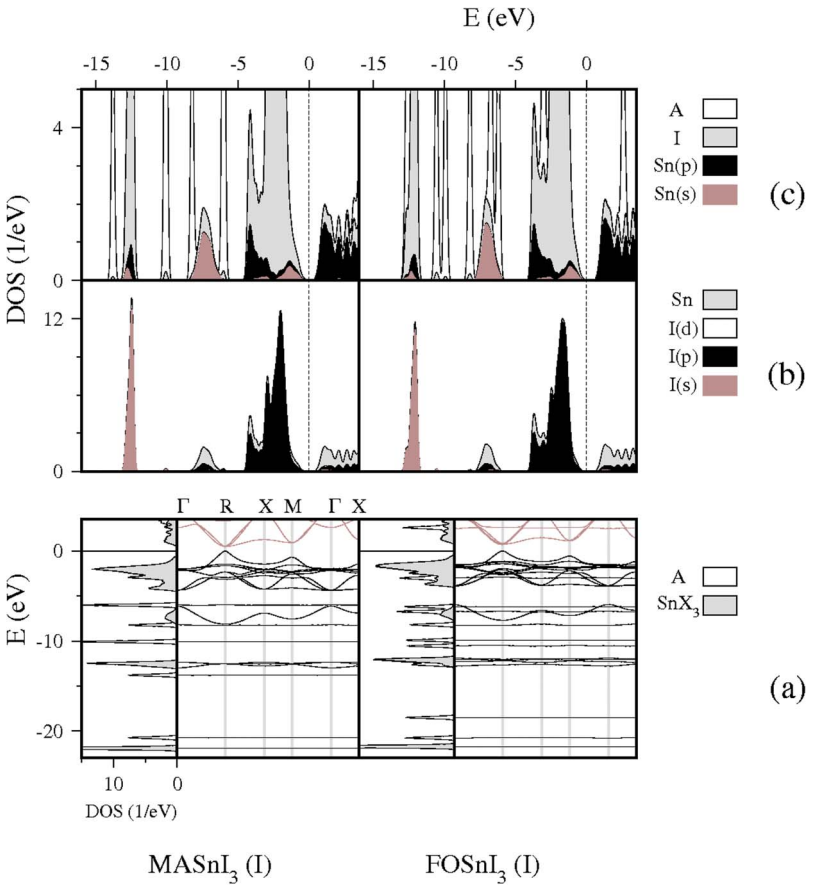


FIG. 11. (Color online) Calculated electronic properties of $MASnI_3$ and $FOSnI_3$: (a) band structure (Ref. 62) and total DOS ; (b) PDOS on Sn (all orbitals), and I *s*, *p*, and *d* orbitals; (c) PDOS on MA or FO (all orbitals), I (all orbitals), and Sn *s* and *p* orbitals. The VBM is arbitrarily set to zero. In (a), the filled (empty) bands are indicated with black (brown) lines. The total DOS (on the left of the band structure) is decomposed into organic (white) and inorganic (brown) contributions.

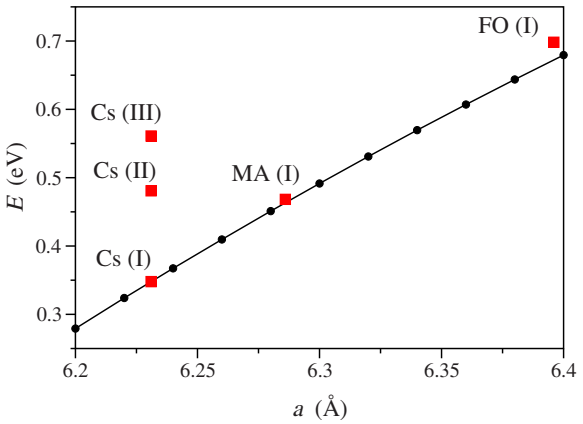


FIG. 12. (Color online) The energy band gap as a function of the cubic lattice $a$. The (black) circles represent the calculated band gap for a perfect cubic perovskite $CsSnI_3$ with different lattice parameters, the black line is intended as a visual guide. The (red) squares represent the band gap of $CsSnI_3$ in the three phases, and the band gap of $MASnI_3$ and of $FOSnI_3$ in the cubic phase.

even if the network is enlarged by the molecule, the compound is characterized by a lower band gap with respect to the inorganic counterpart (in the low-temperature phase).

All these considerations suggest that the electronic properties of tin-halide perovskitic compounds are strongly dependent on the structure of the inorganic cage and, in particular, on the formation of the octahedra network. The molecule thus plays a crucial role because its presence strongly affects the network structure.

## IV. CONCLUSION

In this work, we have given a detailed description of the structural and electronic properties of both inorganic and hybrid perovskites based on tin halides. The comparison between the hybrid perovskites and the inorganic counterparts sheds light on the effects of the molecule on the structural and electronic properties of the compound. Our results show that the electronic properties of tin-halide perovskitic compounds are strongly dependent on the structure of the inorganic cage. In particular, it is found that the structural variation (deformation, tilt, and/or breaking) of the corner-sharing octahedra network strongly affects the band gap of these compounds. The small organic cations (MA and FO) play a crucial role because their presence affects the network structure.

It is important to stress that the size of the molecule must be accurately chosen since the organic molecule must fit into a rigid and relatively small cuboctahedral hole formed by the inorganic cage. Considering that the C-C and C-N bond lengths are of the order of 1.4 Å, it is believed that in the tin-halide based perovskites, only the smallest organic molecules, those containing two or three atoms (excluding hydrogen), should fit into the structure.[4] Larger, more complex monoammonium ($R$-$NH_3^+$) or diammonium ($^+NH_3$-R-$NH_3^+$) cations are indeed used to realize layered organic-inorganic structures.[38,50,51,53,54]

## ACKNOWLEDGMENTS

Financial support from the projects PON STSS-500 and PON S.Co.P.E. is acknowledged. Calculations were performed at CINECA-Bologna ("Progetti Supercalcolo 2007") advanced computing facilities.

*ivo.borriello@na.infn.it

[1] C. Sanchez, B. Julian, P. Belleville, and M. Popall, J. Mater. Chem. **15**, 3559 (2005), and references therein.
[2] P. Gomez-Romero, Adv. Mater. (Weinheim, Ger.) **13**, 163 (2001), and references therein.
[3] F. Mammeri, E. Le Bourhis, L. Rozes, and C. Sanchez, J. Mater. Chem. **15**, 3787 (2005), and references therein.
[4] D. B. Mitzi, Prog. Inorg. Chem. **48**, 1 (1999), and references therein.
[5] S. I. Stupp and P. V. Braun, Science **277**, 1242 (1997).
[6] C. P. Collier, R. J. Saykally, J. J. Shiang, S. E. Henrichs, and J. R. Heath, Science **277**, 1978 (1997).
[7] C. R. Kagan, D. B. Mitzi, and C. D. Dimitrakopoulos, Science **286**, 945 (1999).
[8] D. B. Mitzi, S. Wang, C. A. Feild, C. A. Chess, and A. M. Guloy, Science **267**, 1473 (1995).
[9] D. B. Mitzi, C. A. Feild, W. T. Harrison, and A. M. Guloy, Nature (London) **369**, 467 (1994).
[10] D. B. Mitzi, K. Choundroudis, and C. R. Kagan, IBM J. Res. Dev. **45**, 29 (2001).
[11] J. H. Schön, Ch. Kloc, E. Bucher, and B. Batlogg, Nature (London) **403**, 408 (2000).
[12] M. Grätzel, Nature (London) **414**, 338 (2001).
[13] Y. X. Liu, M. A. Summers, C. Edder, J. M. J. Frechet, and M. D. McGehee, Adv. Mater. (Weinheim, Ger.) **17**, 2960 (2005).
[14] S. E. Shaheen, C. J. Brabec, N. S. Sariciftci, F. Padinger, T. Fromherz, and J. C. Hummelen, Appl. Phys. Lett. **78**, 841 (2001).
[15] J. Takada, H. Awaji, M. Koshioka, A. Nakajima, and W. A. Nevin, Appl. Phys. Lett. **61**, 2184 (1992).
[16] B. Kannan, K. Castelino, and A. Majumdar, Nano Lett. **3**, 1729 (2003).
[17] J. Nelson, Curr. Opin. Solid State Mater. Sci. **6**, 87 (2002).
[18] R. Schroeder and B. Ullrich, Appl. Phys. Lett. **81**, 556 (2002).
[19] F. S. Galasso, *Structure, Properties and Preparation of Perovskite-Type Compounds* (Pergamon, New York, 1969).
[20] D. B. Mitzi, Chem. Mater. **13**, 3283 (2001).
[21] See, for example, K. Yamada, T. Matsui, T. Tsuritani, T. Okuda, and S. Ichiba, Z. Naturforsch., A: Phys. Sci. **45**, 307 (1990); K. Yamada, H. Kawaguchi, T. Matsui, T. Okuda, and S. Ichiba, Bull. Chem. Soc. Jpn. **63**, 2531 (1990).
[22] P. B. R. Vincent, K. N. Robertson, T. S. Cameron, and O. Knop, Can. J. Chem. **65**, 1042 (1987).
[23] S. Wang, D. B. Mitzi, C. A. Feild, and A. Guloy, J. Am. Chem. Soc. **117**, 5297 (1995).
[24] F. Chiarella, A. Zappettini, F. Licci, I. Borriello, G. Cantele, D.

Ninno, A. Cassinese, and R. Vaglio, Phys. Rev. B **77**, 045129 (2008).
[25] A. Poglitsch and D. Weber, J. Chem. Phys. **87**, 6373 (1987).
[26] K. Yamada, S. Nose, T. Umehara, T. Okuda, and S. Ichiba, Bull. Chem. Soc. Jpn. **61**, 4265 (1988).
[27] Y. Furukawa and D. Nakamura, Z. Naturforsch., A: Phys. Sci. **44**, 1122 (1989).
[28] O. Knop, R. E. Wasylishen, M. A. White, T. S. Cameron, and M. J. M. Van Oort, Can. J. Chem. **68**, 412 (1990).
[29] N. Onoda-Yamamuro, T. Matsuo, and H. Suga, J. Phys. Chem. Solids **51**, 1383 (1990).
[30] Q. Xu, T. Eguchi, H. Nakayama, N. Nakamura, and M. Kishita, Z. Naturforsch., A: Phys. Sci. **46**, 240 (1991).
[31] N. Onoda-Yamamuro, T. Matsuo, and H. Suga, J. Chem. Thermodyn. **23**, 987 (1991).
[32] N. Onoda-Yamamuro, O. Yamamuro, T. Matsuo, and H. Suga, J. Phys. Chem. Solids **53**, 277 (1992).
[33] Q. Xu, T. Eguchi, and H. Nakayama, Bull. Chem. Soc. Jpn. **65**, 2264 (1992).
[34] K. Yamada, K. Isobe, T. Okuda, and Y. Furukawa, Z. Naturforsch., A: Phys. Sci. **49**, 258 (1994).
[35] N. Onoda-Yamamuro, O. Yamamuro, T. Matsuo, H. Suga, K. Oikawa, N. Tsuchiya, T. Kamiyama, and H. Asano, Physica B (Amsterdam) **213-214**, 411 (1995).
[36] D. B. Mitzi, C. A. Feild, Z. Schlesinger, and R. B. Laibowitz, J. Solid State Chem. **114**, 159 (1995).
[37] T. Okuda, S. Gotou, T. Takahashi, H. Terao, and K. Yamada, Z. Naturforsch., A: Phys. Sci. **51**, 686 (1996).
[38] I. B. Koutselas, L. Ducasse, and G. C. Papavassiliou, J. Phys.: Condens. Matter **8**, 1217 (1996).
[39] A. Maalej, Y. Abid, A. Kallel, A. Daoud, A. Lautie, and F. Romain, Solid State Commun. **103**, 279 (1997).
[40] H. Ishida, H. Maeda, A. Hirano, Y. Kubozono, and Y. Furukawa, Phys. Status Solidi A **159**, 277 (1997).
[41] D. B. Mitzi and K. Liang, J. Solid State Chem. **134**, 376 (1997).
[42] K. Yamada, Y. Kuranaga, K. Ueda, S. Goto, T. Okuda, and Y. Furukawa, Bull. Chem. Soc. Jpn. **71**, 127 (1998).
[43] A. Maalej, Y. Abid, A. Kallel, A. Daoud, and A. Lutie, Ann. Chim. Sci. Mat. **23**, 241 (1998).
[44] H. Yano, Y. Furukawa, Y. Kuranaga, K. Yamada, and T. Okuda, J. Mol. Struct. **520**, 173 (2000).
[45] D. B. Mitzi, D. R. Medeiros, and P. R. L. Malenfant, Inorg. Chem. **41**, 2134 (2002).
[46] K. Yamada, K. Mikawa, T. Okuda, and K. S. Knight, J. Chem. Soc. Dalton Trans. 2002, 2112.
[47] Y. Lee, D. B. Mitzi, P. W. Barnes, and T. Vogt, Phys. Rev. B **68**, 020103(R) (2003).
[48] I. P. Swainson, R. P. Hammond, C. Soulliere, O. Knop, and W. Massa, J. Solid State Chem. **176**, 97 (2003).
[49] K. Tanaka, T. Takahashi, T. Ban, T. Kondo, K. Uchida, and N. Miura, Solid State Commun. **127**, 619 (2003).
[50] J. L. Knutson, J. D. Martin, and D. M. Mitzi, Inorg. Chem. **44**, 4699 (2005).
[51] M. C. Aragoni, M. Arca, C. Caltagirone, F. A. Devillanova, F. Demartin, A. Garau, F. Isaia, and V. Lippolis, CrystEngComm **7**, 544 (2005).
[52] I. P. Swainson, M. G. Tucker, D. J. Wilson, B. Winkler, and V. Milman, Chem. Mater. **19**, 2401 (2007).
[53] S. Sourisseau, N. Louvain, W. Bi, N. Mercier, D. Rondeau, F. Bouncher, J. Buzare, and C. Legein, Chem. Mater. **19**, 600 (2007).
[54] N. Louvain, W. Bi, N. Mercier, J. Buzare, C. Legein, and G. Corbel, Dalton Trans. 2007, 965.
[55] M. J. Tricker and J. D. Donaldson, Inorg. Chim. Acta **31**, L445 (1978), and references therein.
[56] S. Baroni, A. Dal Corso, S. de Gironcoli, P. Giannozzi, C. Cavazzoni, G. Ballabio, S. Scandolo, G. Chiarotti, P. Focher, A. Pasquarello, K. Laasonen, A. Trave, R. Car, N. Marzari, and A. Kokalj (http://www.quantum-espresso.org).
[57] D. Vanderbilt, Phys. Rev. B **41**, 7892 (1990).
[58] N. Troullier and J. L. Martins, Phys. Rev. B **43**, 1993 (1991).
[59] H. J. Monkhorst and J. D. Pack, Phys. Rev. B **13**, 5188 (1976).
[60] A. M. Glazer, Acta Crystallogr., Sect. B: Struct. Crystallogr. Cryst. Chem. **28**, 3384 (1972), and references therein.
[61] K. Yamada, S. Fuanbiki, H. Horimoto, T. Matsui, T. Okuda, and S. Ichiba, Chem. Lett. **20**, 801 (1991).
[62] The dispersion curves for the different Bravais lattices are shown along the following directions:
(i) orthorhombic:
$$\Gamma(0,0,0) \rightarrow Z\left(0,0,\tfrac{1}{2}\right) \rightarrow T\left(-\tfrac{1}{2},0,\tfrac{1}{2}\right) \rightarrow Y\left(-\tfrac{1}{2},0,0\right) \rightarrow S\left(-\tfrac{1}{2},\tfrac{1}{2},0\right) \rightarrow X\left(0,\tfrac{1}{2},0\right) \rightarrow U\left(0,\tfrac{1}{2},\tfrac{1}{2}\right) \rightarrow R\left(-\tfrac{1}{2},\tfrac{1}{2},\tfrac{1}{2}\right);$$
(ii) tetragonal:
$$\Gamma(0,0,0) \rightarrow X\left(0,\tfrac{1}{2},0\right) \rightarrow M\left(\tfrac{1}{2},\tfrac{1}{2},0\right) \rightarrow \Gamma(0,0,0) \rightarrow Z\left(0,0,\tfrac{1}{2}\right) \rightarrow R\left(0,\tfrac{1}{2},\tfrac{1}{2}\right) \rightarrow A\left(\tfrac{1}{2},\tfrac{1}{2},\tfrac{1}{2}\right) \rightarrow Z\left(0,0,\tfrac{1}{2}\right);$$
(iii) cubic:
$$\Gamma(0,0,0) \rightarrow R\left(\tfrac{1}{2},\tfrac{1}{2},\tfrac{1}{2}\right) \rightarrow X\left(0,\tfrac{1}{2},0\right) \rightarrow M\left(\tfrac{1}{2},\tfrac{1}{2},0\right) \rightarrow \Gamma(0,0,0) \rightarrow X\left(0,\tfrac{1}{2},0\right);$$
(iv) monoclinic:
$$C\left(0,\tfrac{1}{2},\tfrac{1}{2}\right) \rightarrow Y\left(0,\tfrac{1}{2},0\right) \rightarrow \Gamma(0,0,0) \rightarrow B\left(-\tfrac{1}{2},0,0\right) \rightarrow D\left(-\tfrac{1}{2},0,-\tfrac{1}{2}\right) \rightarrow E\left(-\tfrac{1}{2},\tfrac{1}{2},\tfrac{1}{2}\right) \rightarrow A\left(-\tfrac{1}{2},\tfrac{1}{2},0\right) \rightarrow \Gamma(0,0,0) \rightarrow Z\left(0,0,\tfrac{1}{2}\right);$$
and (v) triclinic:
$$\Gamma(0,0,0) \rightarrow Y\left(0,\tfrac{1}{2},0\right) \rightarrow Q\left(0,\tfrac{1}{2},\tfrac{1}{2}\right) \rightarrow Z\left(0,0,\tfrac{1}{2}\right) \rightarrow \Gamma(0,0,0) \rightarrow X\left(\tfrac{1}{2},0,0\right).$$
[63] F. R. Poulsen and S. E. Rasmussen, Acta Chem. Scand. (1947-1973) **24**, 150 (1970).
[64] See, for example, A. M. Glazer, Acta Crystallogr., Sect. A: Cryst. Phys., Diffr., Theor. Gen. Crystallogr. **31**, 756 (1975).